BIOCHEMISTRY
including biophysical chemistry & molecular biology
Article

Biochemistry **2009,** *48,* 5801–5812 5801
DOI: 10.1021/bi900446j

Crucial Role of Asp408 in the Proton Translocation Pathway of Multidrug Transporter AcrB: Evidence from Site-Directed Mutagenesis and Carbodiimide Labeling†

Markus A. Seeger,[‡,§,⊥] Christoph von Ballmoos,[§,@] François Verrey,[‡] and Klaas M. Pos*[,‡,∥]

[‡]*Institute of Physiology and Zurich Centre for Integrative Human Physiology (ZIHP), University of Zurich, Winterthurerstrasse 190, CH-8057 Zurich, Switzerland,* [§]*Institute of Microbiology, Swiss Federal Institute of Technology (ETH), Wolfgang-Pauli-Strasse 10, CH-8093 Zurich, Switzerland, and* [∥]*Cluster of Excellence Frankfurt-Macromolecular Complexes, Institute of Biochemistry, Goethe-University Frankfurt am Main, Max-von-Laue-Strasse 9, D-60438 Frankfurt am Main, Germany* [⊥]*Current address: Institute of Biochemistry, University of Zurich, Winterthurerstr. 190, CH-8057 Zurich, Switzerland.* [@]*Current address: Department of Biochemistry and Biophysics, Arrhenius Laboratories for Natural Sciences, Stockholm University, SE-106 91 Stockholm, Sweden*

Received March 14, 2009; Revised Manuscript Received May 7, 2009

ABSTRACT: The three-component AcrA/AcrB/TolC efflux system of *Escherichia coli* catalyzes the proton motive force-driven extrusion of a variety of cytotoxic compounds. The inner membrane pump component AcrB belongs to the resistance nodulation and cell division (RND) superfamily and is responsible for drug specificity and energy transduction of the entire tripartite efflux system. Systematic mutational analysis of titratable and polar membrane-located amino acids revealed four residues, D407, D408, K940, and, R971, to be of prime importance for AcrB function. Using matrix-assisted laser desorption ionization time-of-flight (MALDI-TOF) mass spectrometry, D408 was shown to specifically react with dicyclohexylcarbodiimide (DCCD) in a pH-dependent manner. The apparent pK_a of D408 of 7.4 would enable binding and release of protons under physiological conditions. In contrast to other secondary transporters, D408 was not protected from carbodiimide modification in the presence of drugs, which supports the notion of spatially separated transport pathways for drugs and protons. This study provides evidence for a substantial role of membrane-located carboxylates as a central element of the proton translocation pathway in AcrB and other members of the RND superfamily.

AcrB, the inner membrane component of the AcrA/AcrB/TolC multidrug efflux system of *Escherichia coli*, is responsible for drug specificity and energy transduction (for reviews, see refs (*1*−*4*)). It belongs to the resistance nodulation and cell division (RND) superfamily and acts as a proton/drug antiporter (*5*). The AcrA/AcrB/TolC efflux pump confers resistance to a variety of antibiotics, dyes, detergents, and bile salts by pumping the substrates from the inner membrane out of the Gram-negative cell bypassing the periplasm (*1*). Loss of any of its three components leads to severe drug sensitivity (*6*, *7*). Several genetic and biochemical studies show that AcrA, AcrB, and TolC form a multiprotein complex (*8*−*14*). Numerous Gram-negative multiresistant clinical isolates (mainly belonging to the Pseudomonads) are associated with a transcriptional upregulation of the AcrA/AcrB/TolC homologous efflux systems (*15*, *16*). The structures of single components of the tripartite AcrA/AcrB/TolC complex from *E. coli* as well as MexA and OprM from *Pseudomonas aeruginosa* have been determined by X-ray crystallography. TolC and OprM are trimeric channels composed of an outer membrane-integrated 40 Å β-barrel domain with an inner diameter of 20 Å which continues as a 100 Å long periplasmic conduit comprising 12 α-helices (*17*, *18*). AcrA and MexA belong to the membrane fusion protein (MFP) superfamily and are postulated to function as a periplasmic adaptor protein connecting AcrB (or MexB) and TolC (or OprM) (*19*). The first structure of homotrimeric RND pump AcrB was obtained at 3.5 Å resolution in a 3-fold symmetrical conformation (*20*−*23*). Recently, an asymmetrical conformational AcrB structure has been determined at 2.5−2.9 Å resolution and is postulated to allegorize the physiologically relevant form (*24*−*26*).

The AcrB monomer contains 12 transmembrane α-helices (TM1−TM12), where TM4 and TM10 are surrounded by the other transmembrane helices of the monomer and harbor the essential residues K940 (TM10) and D407 and D408 (TM4) (*27*, *28*). The periplasmic part of AcrB consists of the TolC docking domain, located most distant from the membrane plane and the porter (formely pore) domain. The TolC docking domain exhibits a 16 Å wide funnel-like structure narrowing from its distal end to a central pore located in the porter domain. The central pore structure consists of three α-helices, each one donated by an AcrB monomer. At the proximal end of the central pore, the structure accommodates a central cavity which extends to a 35 Å wide transmembrane vault defined by the ringlike arrangement of the transmembrane domains of each

†This work was supported by grants of the ETH Zurich, EMDO Stiftung, and the FK of the University of Zurich (to K.M.P.).
*To whom correspondence should be addressed. E-mail: pos@em.uni-frankfurt.de. Phone: 0049 69 798 29251. Fax: 0049 69 798 29201.

 Published on Web 05/08/2009

monomer. Substrate specificity is comprised within the periplasmic part of RND pumps which was shown by domain swapping experiments (*29*−*31*).

The most recent asymmetric structures of AcrB revealed three different conformations of the monomers designated loose (L), tight (T), and open (O) (*24*) or access (A), binding (B), and extrusion (E) (*25*). The three conformations are postulated to represent three consecutive steps of a transport cycle involving the creation of alternate access tunnels to and from a hydrophobic substrate binding pocket within the porter domain. In accordance with functional data (*29*−*32*), minocycline and doxorubicin binding to this hydrophobic pocket in the T or binding monomer could be shown (*25*). It has been postulated that to accomplish drug transport, every monomer cycles through the three conformations (L, T, and O) and thereby provides alternating access to either the cytoplasmic membrane or TolC, ultimately leading to the transport of drugs out of the cell in a fashion similar to that of a peristaltic pump (*2*, *4*, *24*, *25*).

It has been proposed that the transmembrane domain transduces energy from proton translocation to the periplasmic domain to drive the structural conversions of the monomers (*24*). Proton translocation pathways in H^+-coupled membrane proteins include titratable residues which undergo protonation or deprotonation during the transport cycle (*33*−*35*). Spectroscopic features of natural chromophores of, e.g., bacteriorhodopsin or cytochrome *c* oxidase, allowed the determination of pK_a values of key carboxylates. Other methods of determining the proton translocation pathways of transporters, especially those devoid of intrinsic chromophores, include site-directed mutagenesis and biochemical methods that often include the use of hydrophobic carbodiimides such as dicyclohexylcarbodiimide (DCCD),[1] which typically react with key membrane-buried carboxylates of primary and secondary transporters (*36*−*40*). On the basis of site-directed mutagenesis, membrane-located aspartates 407 and 408 were found to be crucial for the function of AcrB and were proposed to play a central role in proton translocation (*27*, *28*). The recently elucidated asymmetric structure of AcrB revealed a prominent side chain movement of K940 within the putative proton translocation site of the O monomer toward D407 and T978 (*24*−*26*). We speculate that protonation and deprotonation events are underlying these conformational changes which trigger the conversion from the T monomer to the O monomer and subsequently to the L monomer. Unlike other secondary active transporters, RND pumps appear to exhibit spatial separation of the proton translocation pathway across the membrane and the drug efflux pathway in the periplasmic portion of the protein. In this report, we show specific modification of aspartate 408 in wild-type AcrB by DCCD using mass spectrometry. In line with separated pathways for protons and drugs, DCCD labeling at aspartate 408 could not be protected in the presence of drugs known to be transported by AcrB. Together with a concomitant detailed site-directed mutagenesis study, we propose a putative proton path through the membrane domain of AcrB.

[1]Abbreviations: ACN, acetonitrile; CHM, cyclohexyl-*n*-hexyl-*β*-D-maltoside; DDM, dodecyl-*β*-D-maltoside; LDAO, lauryldimethylamine *N*-oxide; CNBr, cyanogen bromide; DCCD, *N*,*N*′-dicyclohexylcarbodiimide; MALDI-TOF, matrix-assisted laser desorption ionization time-of-flight; S/N ratio, signal-to-noise ratio.

MATERIALS AND METHODS

Bacterial Strains, Plasmids, and Growth Conditions. Competent *E. coli* DH5α (*41*) and *E. coli* Mach1-T1 (Invitrogen) were used as hosts for cloning procedures (*42*). *E. coli* C43 (DE3) (*43*) harboring pET24acrB$_{His}$ (*21*) was used for AcrB overproduction. The *acrB* knockout *E. coli* BW25113Δ*acrB* strain (*4*) harboring pET24acrB$_{His}$ and mutant derivatives was used for the determination of the minimal inhibitory concentration (MIC). Luria-Bertani (LB) medium and LB agar (*41*) were used for bacterial growth at 37 °C. Kanamycin was used at 50 μg mL^{-1} (Kan^{50}).

Site-Directed Mutagenesis. Mutations were introduced into the *acrB* gene on plasmid pET24acrB$_{His}$ (*21*) using the Quikchange protocol (Stratagene). 5′-phosphorylated oligonucleotides were custom-synthesized by Microsynth (Balgach, Switzerland). All clones were sequenced to ensure the presence of the desired mutation by Microsynth.

Drug Susceptibility Assays. Determination of the MIC was done as follows. Aliquots (1.5 μL) of precultures of *E. coli* BW25113Δ*acrB* carrying pET24acrB$_{His}$ or pET24acrB$_{His}$ containing introduced point mutations in LB Kan^{50} (grown to an OD$_{600}$ between 0.6 and 1 and adjusted to an OD$_{600}$ of 0.6) were used to inoculate LB Kan^{50} (150 μL) with 2-fold serial dilutions of the indicated drug in wells of a 96-well microtiter plate. After incubation (37 °C and 160 rpm) for 22−24 h, the OD$_{600}$ was determined. Control growth without added drugs led to a maximum OD$_{600}$ of 1.8−2.0, and the drug concentration of samples with an OD$_{600}$ of < 0.58 (turbidity visual detection limit) was considered as the minimal inhibitory concentration (MIC). Each assay was repeated at least three times.

Overproduction and Purification of AcrB. Overproduction and purification of AcrB were conducted using cyclohexyl-*n*-hexyl-*β*-D-maltoside (CHM) as a detergent as described previously (*21*, *24*). The eluate (7.5 mL) was concentrated to approximately 8 mg mL^{-1} using an Amicon Ultra 4 centrifugal filter device (100 kDa cutoff, Millipore) spin column.

Carbodiimide Labeling and Sample Preparation for MALDI-TOF Analysis. *N*,*N*′-Dicyclohexylcarbodiimide (DCCD, Fluka) was freshly prepared as a 1 M stock solution in ethanol. If not noted otherwise, purified and concentrated wild-type and mutant AcrB were diluted in 50 mM MES/MOPS (pH 7) containing 0.05% CHM and 0.1% lauryldimethylamine *N*-oxide (LDAO). For DCCD labeling experiments at various pH values, reactions were conducted in 50 mM MES/MOPS/TRICINE (pH 5−9) or in 50 mM MES/MOPS/CHES (pH 9−11), 0.05% CHM, and 0.1% LDAO. The respective pH was adjusted with NaOH. For DCCD labeling experiments with AcrB in different detergents (Figure S1 of the Supporting Information), 0.15% LDAO or 0.05% dodecyl-*β*-D-maltoside (DDM) replaced CHM in the buffers used for AcrB purification. For the evaluation of the possible effects of the *N*-oxide moiety of LDAO, AcrB was purified in CHM and different *N*-oxides were added at a final concentration of 4 mM prior to the DCCD modification reaction. AcrB (0.1 mg mL^{-1}) was labeled at a given concentration of DCCD for a given time in a volume of 100 μL in 96-well polypropylene plates (Nunc) at room temperature. Every modification reaction was conducted in quadruplicate. The labeling reaction was stopped by addition of trichloroacetic acid (TCA, 9.2% final concentration), and the protein was precipitated by centrifugation. Cyanogen bromide (CNBr, Fluka) digestion of the precipitated protein and further

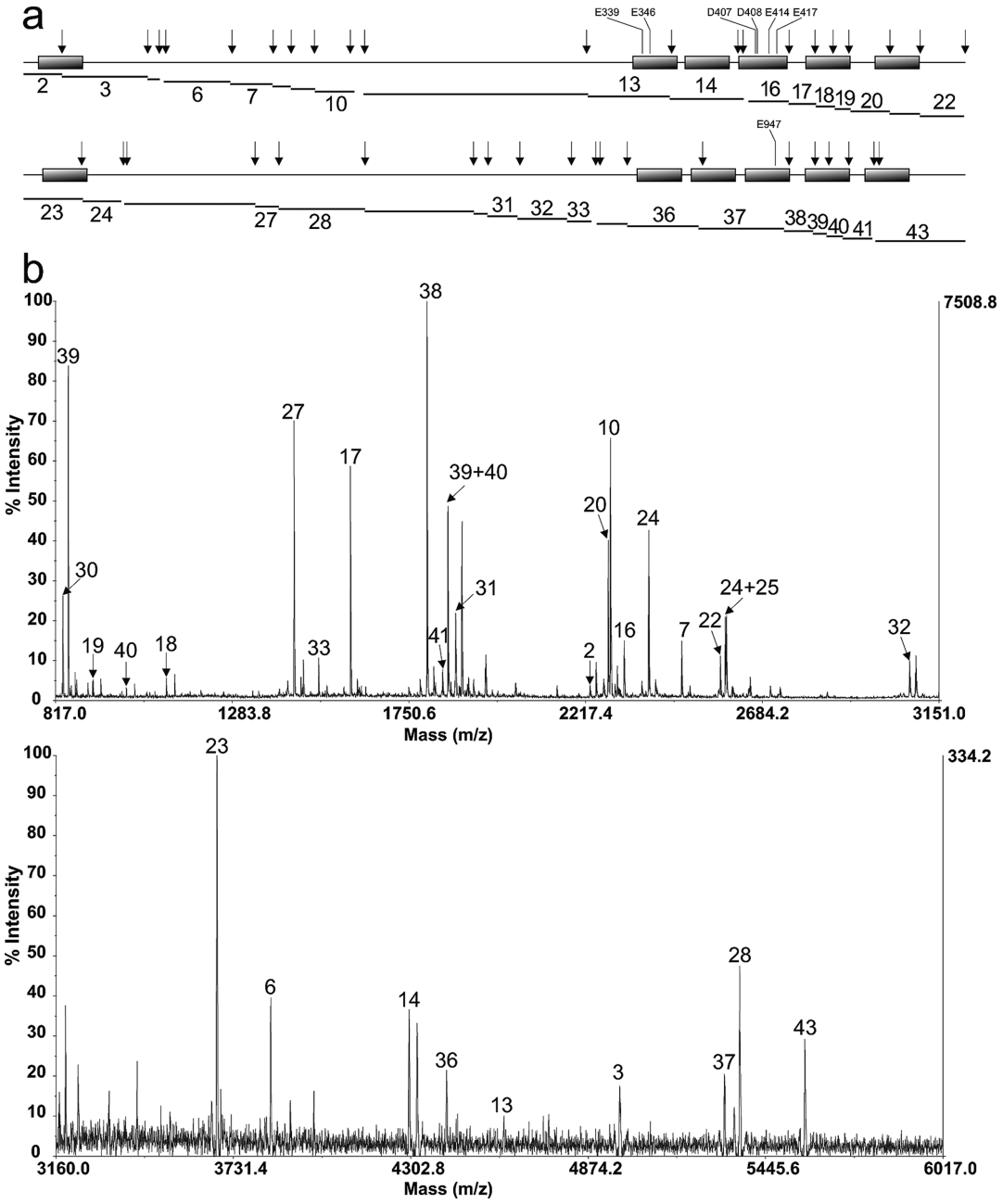

FIGURE 1: MALDI-TOF mass spectrum of CNBr-treated AcrB. (a) Schematic representation of AcrB. The 12 transmembrane helices (rectangles), the CNBr cleavage sites (arrows), and the membrane-located carboxylates are shown. Predicted peptides are indicated by lines and are numbered. (b) Identification of peptides. A typical MALDI-TOF spectrum of CNBr-digested AcrB is shown. Individual CNBr fragments, numbered as depicted in panel a, could be assigned. Twenty-seven of 43 expected peptides, including the peptides harboring the carboxylates of interest, were identified.

sample preparation were carried out as described previously (*44*) with modifications described in ref (*76*). The peptides were dissolved in 80% acetonitrile (ACN) and 0.1% TFA (30 μL), and 1.5 μL was mixed with 10 mg mL^{-1} 2,5-dihydroxybenzoic acid (DHB) in 80% ACN and 0.1% TFA (6 μL). Four times 0.8 μL of the mixture was spotted on a MALDI plate, which was coated with a DHB seed layer. Because each modification reaction was carried out in quadruplicate and the peptides of every digest were spotted four times, 16 MALDI spectra were used for the quantification of one data point.

MALDI-TOF Measurements and Data Analysis. Molecular masses were determined on a 4700 Proteomics Analyzer from Applied Biosystems, a MALDI-TOF instrument equipped with a reflector. All measurements were performed at the Functional Genomics Center Zurich (FGCZ). Some intense peaks observed in the mass spectrum could not be assigned but appeared to be neither due to incomplete CNBr cleavage nor due to partial formylation of serines and threonines, because CNBr digestion was conducted in the presence of TFA instead of the routinely used formic acid. Without the use of ZipTips (see below), the DCCD-labeled peak of peptide 16 could not be observed at a signal-to-noise ratio (S/N ratio) suitable for quantification (Figure 1). Therefore, the S/N ratios of the peak of peptide 16 and the S/N ratios of the nearby peaks of peptides 10, 20, and 24, which originated from the CNBr digest of AcrB, were analyzed (Figure 2). Since the CNBr digest of AcrB was complete, the S/N ratios of the peaks of peptides 10, 20, and 24 served as internal standards. Before data analysis,

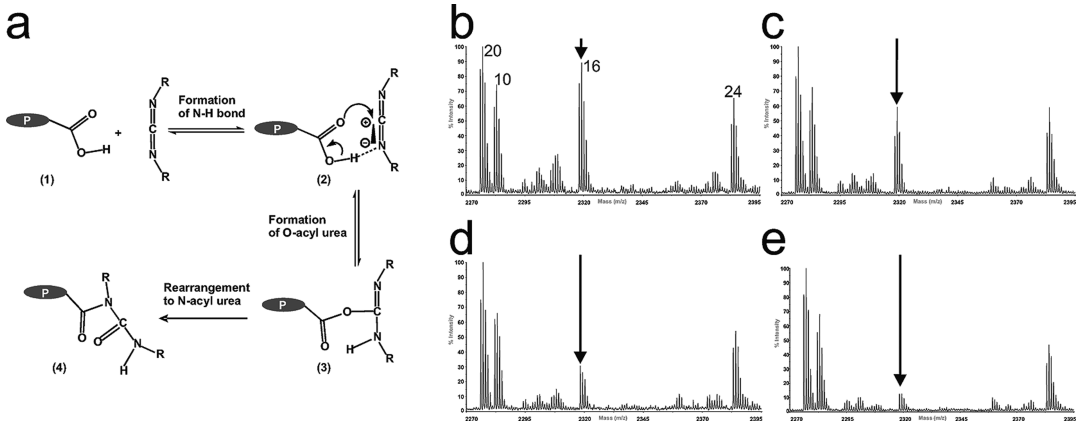

FIGURE 2: (a) Proposed mechanism for the modification of carboxylic acids with DCCD according to Khorana (*46*). In a first step, the carboxylic acid forms a hydrogen bond to one of the nitrogen atoms of the carbodiimide (1). Electron rearrangement leads to the formation of the unstable O-acyl urea derivative (2). In the absence of a nucleophile, rearrangement of the molecule leads to the formation of the stable N-acyl urea derivative (3). (b−e) Time courses of AcrB modification by DCCD. MALDI-TOF spectra of CNBr-digested AcrB incubated for 0 (b), 10 (c), 30 (d), and 60 min (e) with 1 mM DCCD. Disappearance of the peak of peptide 16 containing D407 and D408 (arrow) relative to the three intrinsic neighboring calibration peaks of peptides 10, 20, and 24 (see Figure 1) was observed. DCCD modification was quantified by comparing the S/N ratio of the peak of peptide 16 with the S/N ratios of peaks 10, 20, and 24.

the quality of each spectrum of a data set (typically 96−192 spectra on the same MALDI plate) was assessed according to the peak intensities and the relative ratios of the internal standard peptides to systematically eliminate outliers. Within a data set, the average S/N ratios of the three internal standard peaks were calculated. Spectra exhibiting S/N ratios of internal standard peaks less than one-third of the respective average S/N ratio were omitted. For every spectrum in a data set, quotients of the S/N ratios of peptides 10 and 20 and of peptides 24 and 20 were calculated. These two quotients are expected to be constant within a data set, and large deviations indicated a bad quality spectrum. The averages of these two quotients were calculated within a data set, and every spectrum deviating more than 30% in at least one of the quotients was discarded. Applying these two quality criteria, we omitted approximately 25% of the spectra of every data set. In every remaining spectrum, the S/N ratio of the peptide 16 peak was compared with the sum of the S/N ratios of the three internal standard peaks. The quotient corresponding to the zero point of DCCD labeling curves was determined by CNBr digestion and MALDI-TOF analysis of unlabeled AcrB (S/N ratio of peptide 16 peak high relative to the internal standard peaks). Complete DCCD labeling (100%) was achieved, when the peptide 16 peak was below the detection limit. The degree of DCCD modification was calculated from every spectrum. Subsequently, the numbers for every independent DCCD modification reaction and CNBr digest (represented by four spectra) were averaged. Every data point in the graphs consists of four independent DCCD modification reactions and CNBr digests (representing maximally 16 spectra, but typically 12 spectra due to the systematic omission of low-quality spectra; see above). Hence, the averages and the standard deviations of the above averaged numbers of the four independent DCCD modification reactions and CNBr digests were calculated for every data point. For the determination of the pK_a value of the labeled residues, the degree of modification of peptide 16 as a function of the pH was fitted to the following equation:

$$Y = \frac{a}{1 + \frac{e^{-(X - X_0)}}{b}}$$

where a, b, and X_0 represent the highest value of the fit, the lowest value of the fit, and the pK_a, respectively.

MALDI-TOF/TOF Measurements. We encountered difficulties detecting DCCD-modified peptide 16 after CNBr digestion of AcrB. This could be due to unspecific binding of DCCD-modified peptide 16 to surfaces (e.g., of plastic tubes) and/or decreased ionization efficiency during the MALDI-TOF measurement compared to that for unmodified peptide 16. To prevent the first, CNBr digestion was conducted in glass vials. Wild-type AcrB and the mutants D407N and D408N (10 μg each) were labeled with 1 mM DCCD for 1 h in 50 mM MES/MOPS (pH 7) containing 0.05% CHM and 0.1% LDAO. After the usual digestion procedure, the peptides were dissolved in 30% ACN and 0.1% TFA (10 μL). Peptides were loaded on ZipTips (Millipore) containing C_{18} reversed phase resins, which were prepared according to the manufacturer's protocol. The high ACN concentration of 30% allowed the enrichment of the hydrophobic peptides, including DCCD-modified peptide 16 on the resin. The ZipTips were washed with 50% ACN and 0.1% TFA (4 × 10 μL), and the peptides were eluted with 90% ACN and 0.1% TFA (4 μL) directly onto the prespotted crystalline DHB matrix. MALDI-TOF/TOF analysis was performed under standard conditions using argon as the collision gas. We observed decomposition of DCCD during analysis, most likely as a result from high laser intensities, which are required to induce peptide fragmentation during MALDI-TOF/TOF measurements. Similar defragmentation patterns were observed in DCCD-labeled
c-monomers of ATP synthase (*45*). We therefore used the m/z of the peptide labeled with the decomposed DCCD (m/z 2399.29 ± 0.5) as the parent ion for MALDI-TOF/TOF sequencing.

RESULTS

Identification of DCCD-Modified CNBr-Digested Peptide Fragments by MALDI-TOF Mass Spectrometry. We investigated the reaction of the carbodiimide DCCD on the secondary proton/drug antiporter AcrB. Carbodiimides specifically react with protonated acidic residues in hydrophobic environments (Figure 2a) (*38*, *46*). According to the AcrB structure (Protein Data Bank entry 2GIF), three carboxylates (E346, D407, and D408) are deeply buried in the transmembrane domain while four other carboxylates (E339, E414, E417, and E947) located near the putative membrane−solvent boundary.

In a first experiment, carbodiimide labeling was observed after incubation of AcrB with [^{14}C] DCCD followed by SDS−PAGE and autoradiography (not shown). To assign the carbodiimide labeling to (a) specific carboxylate(s), DCCD-modified AcrB was digested and the resulting peptides were analyzed by MALDI-TOF mass spectrometry. Initial attempts to analyze tryptic digests of DCCD-treated AcrB failed due to poor sequence coverage of the membrane domain. With CNBr digestion, complete cleavage could be attained (except when methionine was followed by serine or threonine) and the obtained peptides were well-suited for MALDI-TOF mass spectrometry measurements (Figure 1). Out of the 43 in silico predicted peptides, 27 could be identified and were numbered according to the series of predicted CNBr cleavage products. From the 16 peptides which could not be identified, 11 could not be measured due to molecular mass restrictions (< 800 or > 6000 Da), and five peptides could not be detected due to unknown reasons. Of the 42 methionines in the AcrB sequence, six are followed by either serine or threonine, causing incomplete CNBr cleavage due to conversion of methionine to homoserine (*47*). Two homoserine-containing peptides resulting from this side reaction could be detected (peptides 24 + 25 and 39 + 40 in Figure 1). Importantly, peptides containing the carboxylates of interest, i.e., peptide 13 (4745 Da; E339 and E346), peptide 16 (2318 Da; D407, D408, E414, and E417), and peptide 37 (5311 Da; E947), could clearly be assigned. The peak intensity of peptide 13 (harboring E339 and E346) was rather low, but when the spectrum was recorded in linear mode by MALDI-TOF, the signal markedly improved (not shown).

Identification of D408 as the Main DCCD Reactive Carboxylate. Of the three peptides of interest (13, 16, and 37), we identified peptide 16 (^{399}VLAIGLLV**DD**AIVVV**E**N-V**E**RVh^{420}, 2524.66 Da) originating from transmembrane helix 4 and including the functionally essential residues D407 and D408 to react specifically with DCCD. DCCD-modified peptide 16 could be detected reproducibly only by MALDI-TOF after the hydrophobic CNBr-digested peptides were enriched on reversed phase resin of C18 ZipTips (see Materials and Methods). Importantly, multiple DCCD labeling of peptide 16 was not detected (not shown). Further analysis of the DCCD-modified peptide 16 by tandem mass spectrometry revealed that the mass of the y_{13} ion (^{408}**D**AIVVV**E**NV**E**RVh^{420}) was increased by 81.06 Da (designated y_{13}* in Figure 3, bottom panel), whereas the peak representing the unmodified y_{13} ion was absent (Figure 3). Due to the lack of the latter y ion in the spectrum, it was concluded that D408 (and to a minor extent also E414 and E417), but not D407, is the site of DCCD modification in wild-type AcrB. The mass increase of the y_{13}* ion by 81.06 Da was less than the calculated increase of 206.18 Da upon DCCD modification. This phenomenon has previously been described as resulting from fragmentation of the attached DCCD during the recording of the MALDI-TOF/TOF spectrum, for which a higher laser intensity was required compared to that for the measurement of the MALDI-TOF spectrum (*45*). Although E414 and E417 are labeled with DCCD as well, the respective y_6* and y_{12}* ions are highly overrepresented in the spectrum due to an enhanced cleavage effect (*48*), a finding which is in agreement with the negligible DCCD labeling of the D407N/D408N double mutant (Figure 4b). A full interpretation of the MALDI-TOF/TOF spectra is given in the legend of Figure 1 of the Supporting Information.

DCCD Labeling Occurs in a Concentration- and Time-Dependent Manner. To address the carbodiimide modification

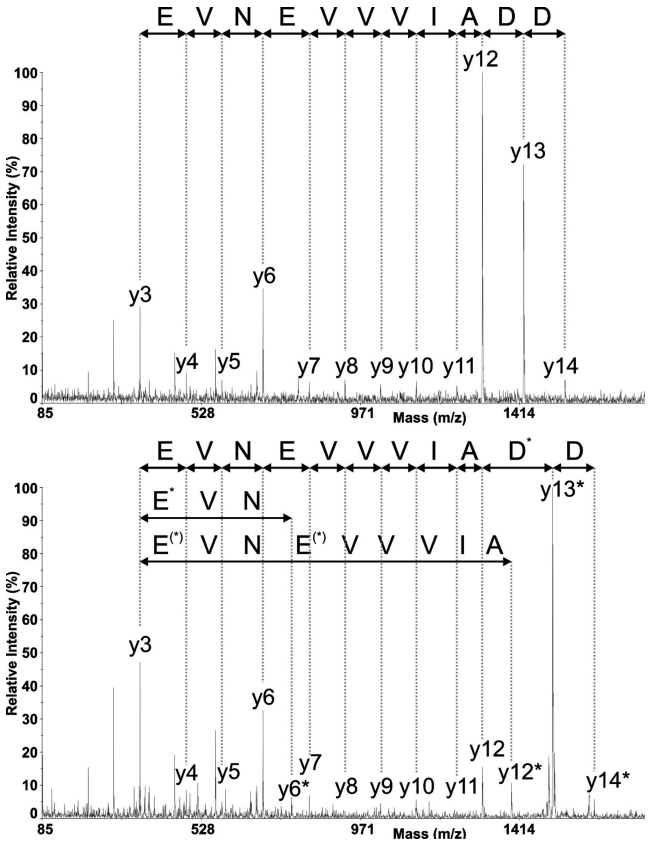

FIGURE 3: MALDI-TOF/TOF mass spectrometry analysis of unmodified (top panel) and DCCD-modified (bottom panel) peptide 16 of wild-type AcrB. The detected peaks of the y ion series are indicated. DCCD-modified y ions (resulting in a mass increase of 81.06 Da) are denoted with asterisks.

of peptide 16 as a function of DCCD concentration and reaction time, CNBr-digested AcrB peptides were analyzed in a high-throughput manner without the optional ZipTip enrichment (due to practical and economical reasons). Without the ZipTip procedure, detection of the modified peptide was difficult; however, the reduction of the signal of the unlabeled peak of peptide 16 (2318 Da) could easily be traced. The signals of the nearby CNBr peptide peaks of peptides 10 (2282 Da), 20 (2276 Da), and 24 (2383 Da) derived from complete CNBr digestion of AcrB, served as internal standards, and allowed calculation of the degree of carbodiimide modification of peptide 16 (Figure 2b−e).

To determine the optimal DCCD concentration for subsequent experiments, wild-type AcrB was incubated with different DCCD concentrations ranging from 200 μM to 4 mM for 60 min at pH 7 (Figure 4a). At a DCCD concentration of 1 mM, ~80% carbodiimide modification was achieved and the degree of labeling did not markedly increase using 2 or 4 mM DCCD for this given time period. We therefore used DCCD at a concentration of 1 mM for all following experiments, which is within the concentration range used for other carbodiimide modification studies on secondary transporters (*39*, *40*).

Among the four possible carboxylates of peptide 16, only D407 and D408 have been reported to play a pivotal role in the proton translocation of AcrB (*20*, *28*) and D408 was shown to be the main DCCD-reactive carboxylate by tandem mass spectrometry. Therefore, time-dependent DCCD modification of mutants D407N, D408N, and D407N/D408N was compared to the modification of the wild-type protein at pH 7 (Figure 4b). A slight decrease in the DCCD modification rate was observed for

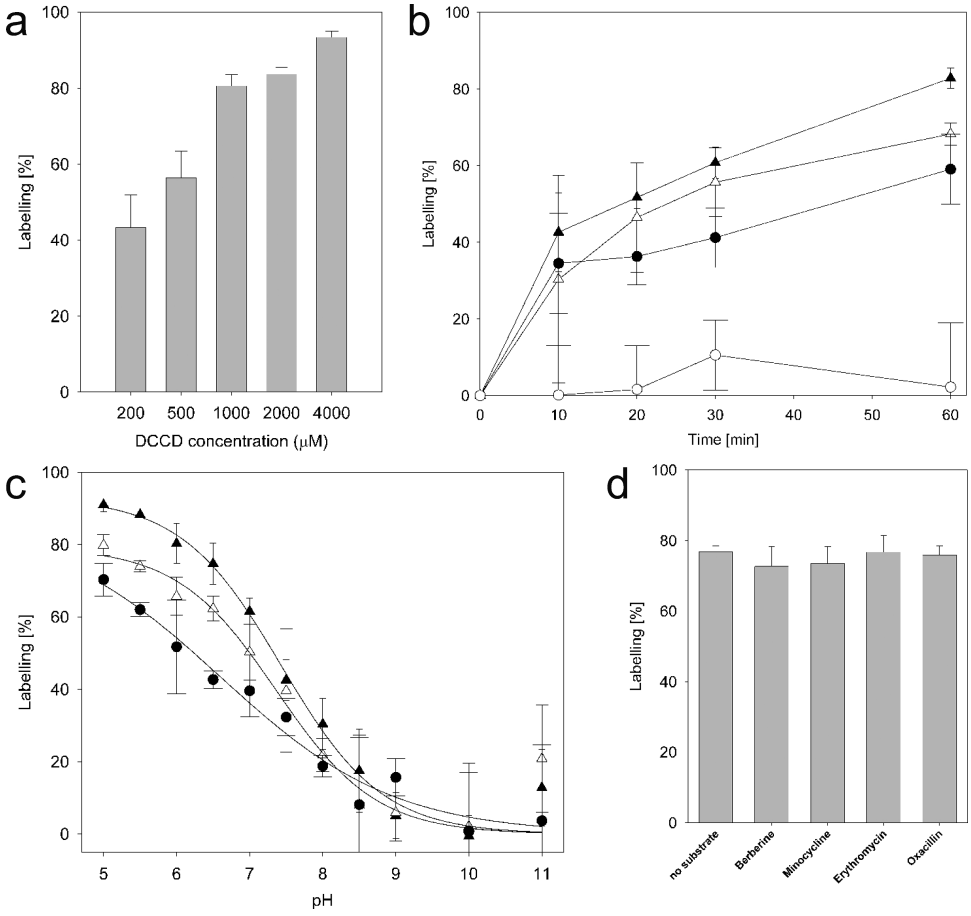

FIGURE 4: Rate of carbodiimide modification of peptide 16 as a function of DCCD concentration and pH. (a) Wild-type AcrB was labeled with various DCCD concentrations at pH 7 for 60 min. (b) Time-dependent carbodiimide modification of wild-type AcrB (▲) and the mutants D407N (△), D408N (●), and D407N/D408N (○) in the presence of 1 mM DCCD at pH 7. (c) Extent of DCCD modification of wild-type AcrB (▲) and mutants D407N (△) and D408N (●) as a function of pH. AcrB was incubated for 30 min with 1 mM DCCD between pH 5 and 11. Sigmoidal curves were fitted through the data points (see Materials and Methods). Also shown are the standard deviations. (d) DCCD modification of AcrB in the absence or presence of substrates. Wild-type AcrB was incubated with 1 mM DCCD for 30 min at pH 7 in the absence or presence of the indicated substrates at 1 mM.

both the D407N and D408N mutants, whereas for double mutant D407N/D408N, almost no carbodiimide modification was detected. This result supports the notion that E414 and E417 are barely labeled with DCCD in the wild-type protein.

MALDI-TOF/TOF Analysis of the D408N and D407N Mutants. D408 was identified as dominant carbodiimide reactive carboxylate in the AcrB wild-type protein (Figure 3a). Since the D408N AcrB mutant is also reactive toward DCCD (Figure 3b), the question of which carboxylate of the D408N mutant was modified arose. The MALDI-TOF/TOF spectrum of DCCD-labeled peak 16 of the D408N mutant shows that mainly D407 and also, but to a smaller extent, E417 and E414 are modified by DCCD (Figure 1c of the Supporting Information).

The MALDI-TOF/TOF spectrum of DCCD-labeled peptide 16 (^{399}VLAIGLLV**ND**AIVVV**E**NV**E**RVh^{420}) of the D407N AcrB mutant confirmed that D408 is the major site of modification in this mutant (Figure 1b of the Supporting Information).

pH Profile of DCCD Modification. Since carbodiimides react specifically with protonated carboxyl groups (Figure 2a), an apparent pK_a of the reacting side chain(s) can be approximated by studying reactivity as a function of pH (*49*, *50*). Wild-type and mutant AcrB were incubated with 1 mM DCCD for 30 min in polybuffer (see Materials and Methods) between pH 5 and 12 (Figure 4c). The degree of modification of peptide 16 as a function of pH was fitted to a sigmoidal equation (see Materials and Methods). The inflection point of the fitted curve reflects the pK_a of the labeled residue(s). For both the wild type and the D407N mutant, a pK_a of 7.4 was obtained. In contrast, the pK_a detected for the D408N mutant was shifted toward the acidic by almost 1 pH unit at 6.6. This difference should, however, be taken with considerable care because of the large standard deviations observed with the data points originating from the measurements at pH ≥7 (Figure 4c). At low pH values, the velocity of DCCD labeling was markedly slower for the D407N and D408N mutant compared to that of the wild type. The observed pK_a value for D408 is up to 3 pH units higher than one would expect for carboxylic acid residues in solution. These results are indicative of the essential role of D408 and also D407 in protonation/deprotonation events at physiological pH.

Substrates Do Not Influence Carbodiimide Modification. For secondary transporters like the proton/lactose symporter LacY and the drug/proton antiporter EmrE, it has been shown that their cognate substrates protect against DCCD labeling (*39*, *40*). To study potential protection by substrates against DCCD modification of D408, wild-type AcrB was incubated with 1 mM DCCD for 30 min in the presence of either berberine, minocycline, erythromycin (all positively charged), or oxacillin (negatively charged), each at 1 mM (Figure 4d). Clearly, the presence of the added substrates did not significantly affect the extent of DCCD labeling, which implies either a spatial

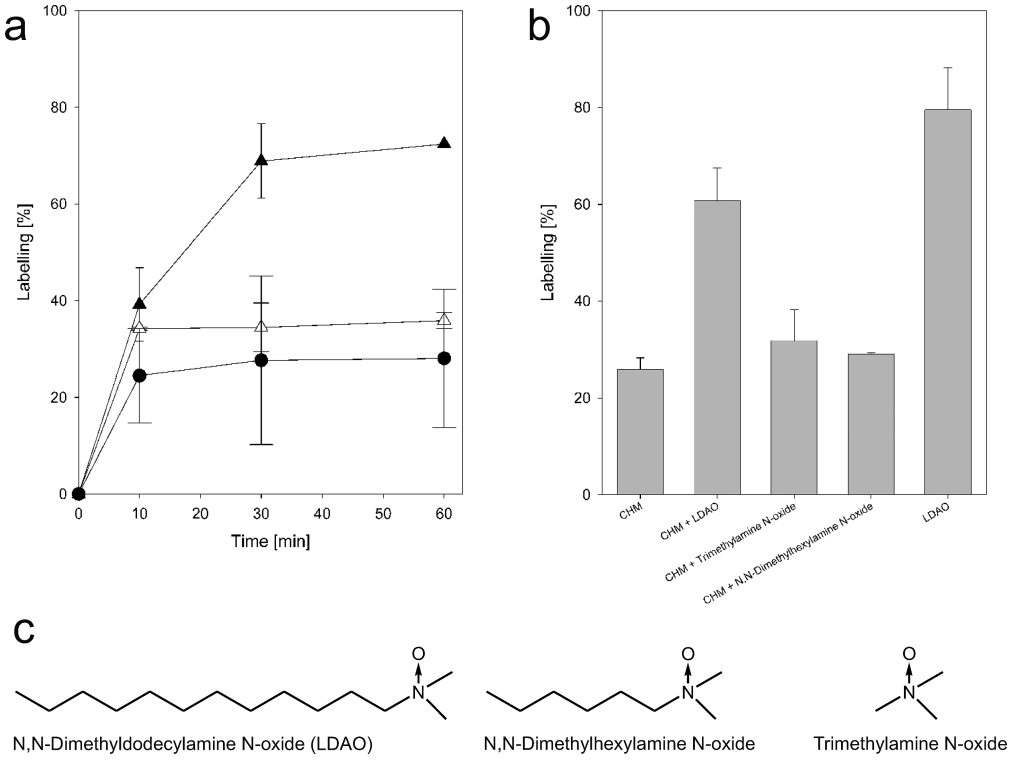

FIGURE 5: Effect of LDAO on the extent of DCCD labeling of AcrB. (a) Time-dependent labeling of wild-type AcrB purified and kept in LDAO [0.15% (▲)], CHM [0.05% (△)], and DDM [0.05% (●)] in the presence of 500 μM DCCD (pH 7). (b) Extent of DCCD labeling of AcrB in the absence or presence of *N*-oxide detergents. The possible effect of the *N*-oxide moiety was checked by labeling of wild-type AcrB with 1 mM DCCD for 60 min at pH 7. AcrB was purified in the presence of CHM, and *N*-oxide (final concentration of 4 mM) was added prior to DCCD incubation. As a control, AcrB purified in the presence of LDAO was used. (c) Chemical formula of the *N*-oxides used in panel b.

separation of the substrate and proton translocation pathways or a rather low substrate affinity of AcrB within this experimental setup to detect protection. Notably, minocycline (used at a concentration of 2.4 mM) is bound to the hydrophobic pocket of the AcrB T monomer's porter domain as shown by X-ray crystallography under similar buffer conditions (*25*). Moreover, recent substrate−AcrB binding studies with detergent-solubilized protein showed rather high binding affinities of 5−74 μM (*51*).

Addition of LDAO Prevents Precipitation of AcrB and Increases the Degree of Labeling. DCCD labeling of AcrB in the presence of DDM or CHM (final concentration of 0.05%) reproducibly attained maximal values to 30%, which could be increased to 80% by the addition of 0.1% LDAO (Figure 5). Gel filtration chromatography of AcrB in the presence of CHM or DDM indicated severe aggregation on exposure to DCCD (not shown), which was interpreted as a possible cause for the low maximal extent of modification of approximately 30%. The addition of LDAO (final concentration of 0.1%) to AcrB purified initially in CHM (0.05%) markedly reduced the amount of aggregation caused by DCCD. The samples in the presence of LDAO were characterized by a high degree of monodispersity (not shown) and a high degree of modification after exposure to DCCD (Figure 5). A possible explanation of the beneficial effect of LDAO on DCCD labeling could be a direct interaction of the *N*-oxide zwitterionic moiety with aspartate 407 and/or 408. Unlike LDAO, however, the addition of trimethylamine *N*-oxide or *N*,*N*-dimethylhexylamine *N*-oxide did not increase the degree of DCCD labeling (Figure 5b,c). Although the lack of a long aliphatic moiety of the latter *N*-oxides might prevent accessibility to D407 and D408, we interpret the effect of LDAO as protection of AcrB from aggregation due to its properties as a detergent (enabling continuation of the labeling reaction), rather than to interact with the membrane-embedded carboxylates via its *N*-oxide moiety.

Mutational Analysis of the Putative Proton Translocation Site. In the O (extrusion) monomer of the asymmetric AcrB structure (Protein Data Bank entry 2GIF), the side chain orientation of K940 (TM10) relative to D408 and D407 (both on TM4) is markedly different from the local conformation in the L and T monomers (Figure 6). The differences in side chain conformation are believed to reflect different states of protonation and deprotonation leading to the structural conversion of the subdomains inside the periplasmic porter domain (*24*, *25*). The specific pH-dependent carbodiimide modification of D408 in the AcrB wild-type protein puts further emphasis on the physiological role of this membrane-buried charge network. On the basis of mutagenesis studies, the residues of the triad of D407, D408, and K940 are postulated to play a central role in the proton translocation pathway of the AcrB homologue MexB of *P. aeruginosa* (*27*). A mutational study on the proton translocation pathway of AcrB was recently reported, including an alanine scanning mutagenesis of all membrane-located titratable and polar residues (*28*). Substitutions D407A, D408A, K940A, T978A, and R971A caused almost complete inhibition of the AcrB-catalyzed resistance toward cholate. In this study, we substituted D407 and D408 with asparagine and glutamate, K940 with arginine, histidine, alanine, and methionine, and other residues with possible roles in proton translocation (as deduced from the 2GIF structure) with alanine. Table 1 summarizes the minimal inhibitory concentration (MIC) of the six structurally unrelated drugs tetraphenylphosphonium, oxacillin, rhodamine 6G, berberine, erythromycin, and linezolid for *E. coli* BW25113ΔacrB producing wild-type AcrB or AcrB mutants. Western blot analysis revealed that the wild type and all AcrB

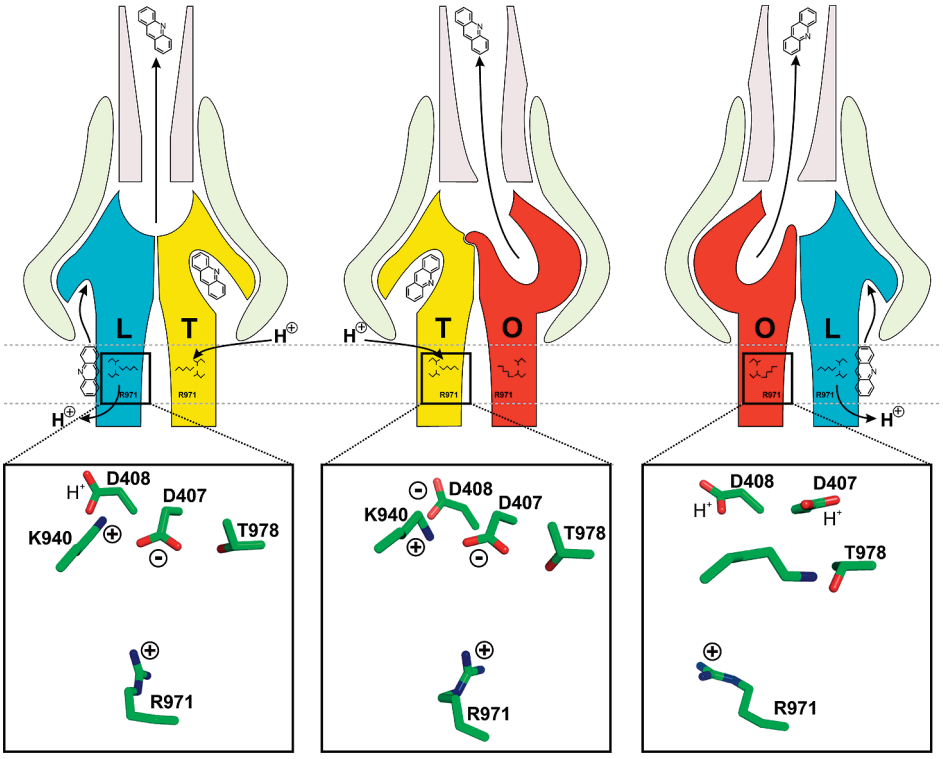

FIGURE 6: Schematic representation of the AcrB alternating site functional rotation transport mechanism. The conformational states loose (L), tight (T), and open (O) are colored blue, yellow, and red, respectively. Only the side views of two of the three monomers of the AcrB trimer are shown. AcrA and TolC are colored light green and gray, respectively. The proposed proton translocation site (D407, D408, and K940) is indicated in the membrane part of each monomer. In the first state of the cycle (from left to right), a monomer binds a substrate (acridine) at its transmembrane domain (L conformation); subsequently, the substrate enters the hydrophobic binding pocket (T conformation), and finally, the substrate is released to the funnel toward TolC (O conformation). The conversion from the T monomer to the O monomer conformation is suggested to be the major energy-requiring (proton motive force-dependent) step in this functional rotation cycle and presumably requires the binding of a proton to the proton translocation site (D407, D408, and K940) from the periplasm. The release of a proton from the proton translocation site to the cytoplasm might occur during conversion from the L monomer to the T monomer. Alternatively, R971 might be deprotonated in the L monomer and proton release would then occur during the O to L transition (*4*, *74*). AcrA is expected to participate in the transduction of the conformational changes from AcrB to TolC, which results in movement of the TolC distal subdomain and the facilitation of drug extrusion to the outside of the cell.

mutants were synthesized as indicated by the presence of a major α-AcrB immunoreactive band with an electrophoretic mobility corresponding to a protein of ~110 kDa (Figure 2 of the Supporting Information). The level of production of mutants D407E and R418A was lower compared to those of the other mutants, but because mutant R418A was fully active (Table 1), the observed decrease in the level of production hardly seems to affect transport activity. Moreover, misfolding of mutant protein can be excluded for several mutants because overproduction, purification, and crystallization yielded well-diffracting crystals (not shown). The D407N substitution leads to a complete loss of function. Interestingly, a small reproducible residual activity could be observed for the D408N mutant. Substitution of the key aspartates D407 and D408 with glutamate resulted in a substantial loss of activity, but some activity remained. The length of the titratable side chain seems to be critical, similar to the situation for the key carboxylates D61 of *E. coli* F_1F_o ATP synthase (*36*) and E269 of LacY (*52*). Notably, whereas the effect of D407E or D408E substitution on AcrB function was approximately the same, these mutants in the *P. aeruginosa* homologue MexB caused a more differentiated MIC pattern, D408E being more active than D407E (*27*). The presumably positive charge on the primary amine group of K940 seems to be very important. This residue could be substituted with arginine without losing drug efflux activity, and also mutant K940H showed residual activity comparable to the activity of the D407E and D408E mutants (Table 1). Mutants harboring substitutions lacking an amine group like K940A and K940M were not able to confer resistance. Notably, the double mutants D407E/K940R and D408E/K940R exhibited MIC values higher than those of the single glutamate mutants, the latter double mutant being slightly more active than the D407E/K940R mutant (Table 1). On the other hand, double mutants D407E/K940H and D408E/K940H exhibited no activity. From these results, it can be concluded that carboxylic acid (at positions 407 and 408) and amine residues (at position 940) appear to be essential for the function of AcrB.

Polar Residues Flanking the Triad. Three polar residues S481, N941, and T978 are within hydrogen bonding range of the essential residues D407, D408, and K940. All these residues are highly conserved within the hydrophobe/amphiphile efflux-1 (HAE-1) family (*53*). Substitutions N941A and S481A resulted in an only minor decrease in MIC (Table 1). However, mutant T978A conferred a considerable decrease (but was not completely inactivated) in resistance to all drugs tested. A D407E/T978A double mutant, however, completely abolished the drug resistance phenotype. The results are in full agreement with former activity measurements of the N941A, S481A, and T978A AcrB mutants using cholate as a substrate (*28*). The high degree of conservation of T978 among the RND superfamily members suggested a critical role for this residue in drug efflux activity. In the L and T monomer, the hydroxyl group of T978 on TM11 possibly interacts with D407 since it is within 2.8 Å. In the O

Table 1: Drug Resistance of *E. coli* BW25113Δ*acrB* Expressing *acrB* Mutant Genes from Plasmid pET24acrB$_{His}$[a]

	tetraphenylphosphonium	oxacillin	rhodamine 6G	berberine	erythromycin	linezolid
plasmid[b]						
pET24a	12.5	2−4	4−8	128	2−4	8−16
pET24acrB$_{His}$	800	128	256	2048	64	256
mutation						
triad						
D407N	12.5	2−4	4−8	128	2	8−16
D407E	50	16	16−32	256	4	16
D408N	12.5−25	4−8	8	128	4	8−16
D408E	50	8−16	32	256	4	16
K940R	400	128	128	1024	64	128
K940H	50	8−16	32	256	4−8	16
K940A	12.5	4	8−16	128	4	8−16
K940M	12.5	2−4	4−8	64−128	2−4	8
D407E/K940R	100	32	32−64	256	8	32
D407E/K940H	12.5	2−4	8	128	4−8	8−16
D408E/K940R	200	64	64	256	16	64
D408E/K940H	12.5	4−8	8	128	4−8	16
S481A	400	64−128	64	512	64	128
N941A	800	64−128	128−256	1024	64	128−256
T978A	25−50	16	64	256	8−16	32
D407E/T978A	12.5	2−4	4−8	128	4	8
periplasm to triad						
T933A	800	128	256	2048	64	256
T1015A	800	64−128	256	1024	64	128
triad to cytoplasm						
E414Q	200	64−128	128	1024	64	32
E417Q	400	128	128−256	1024	64	128
R418A	800	64−128	256	2048	64	128
R971A	12.5	4	4	128	4	8

[a] Each assay was repeated at least three times. [b] *E. coli* BW25113Δ*acrB* cells harboring pET24aHis or pET24acrBHis encoding AcrB were used as a negative or positive control, respectively.

monomer, K940 comes within 2.8 Å of T978 and N941 and might therefore be involved in hydrogen bonding (*24*). The role of T978 has to be put into perspective, however, since substitution with non-hydrogen bond donor side chains like valine and isoleucine still produces functional AcrB (*28*).

Hydrophobic Barrier. Uptake of protons from the periplasm and release of protons toward the cytoplasm are anticipated in a proton motive force-dependent symport or antiport process. Critical residues involved in proton binding and release like E14 in EmrE, E269 in LacY, and D407/D408 in AcrB have thus to be reached by protons from the periplasm. In the case of LacY (*54*), evidence has accumulated that the proton binding sites are accessible through the bulk water via an alternate access mechanism. In AcrB, a number of titratable and polar residues are situated between the D407/D408/K940 triad and the cytoplasm. In contrast, only a few polar residues are found in the region from the periplasm toward the triad. Polar residues might be involved in coordinating water molecules involved in proton transport. A putative proton pathway from the periplasm toward the proton relay triad could involve residues T934, S938, N941, and T1015 located on TM9, TM10, and TM12. Among those four residues, N941 and T1015 are the most conserved, but both N941A and T1015A mutants are functionally active (Table 1). Another pathway from the periplasm to the triad involves T933, but again a T933A mutant yields wild-type MIC values. The findings confirm results published recently (*28*). It shows that the pathway from the periplasm to the D407/D408/K940 triad remains elusive and would benefit from a high-resolution structure of AcrB for visualizing structured waters inside the transmembrane region.

The Proton Path Involves R971. Several conserved titratable residues are located between the D407/D408/K940 proton translocation site and the cytoplasm. Likely candidates are E414, E417, R418, and R971. Substitution of E417 with glutamine was almost without effect on activity (Table 1), despite strong conservation between transporters of the RND superfamily and even between the RND and ABC superfamilies (*55*). Similarly, substitution of R418 with alanine only slightly decreased the activity of AcrB. In contrast, the E414Q mutant showed a strongly reduced activity toward tetraphenylphosphonium and linezolid, whereas it remains highly or fully active toward oxacillin, berberine, rhodamine 6G, and erythromycin (Table 1). This pattern appears atypical for a residue thought to be involved in proton transport and might suggest a direct interaction between some of the drugs and E414. Very recently, a similar phenomenon has been described for a mutant in the ABC cassette of multidrug ABC transporter Pdr5 expected to reduce ATPase activity, which had a major impact on rhodamine transport while leaving the transport activity for other drugs and the steady state ATP hydrolysis rate unaffected (*56*). The role of E414 could be similar to that of E204 of bacteriorhodopsin, which is an important residue at the membrane boundary not directly involved in protonation and deprotonation but postulated to build a crucial part of a hydrogen-bonded network responsible for proton transport (*57*). Noteworthy, in the RND cation/proton antiporter CzcA, the E414Q (AcrB numbering) substitution completely abolishes ion transport (*58*).

The R971A substitution leads to a complete loss of function for all tested substrates (Table 1) as reported previously (*28*, *59*). Hence, R971, D407, D408, and K940 appear to be absolutely

necessary for function. Activity loss was not due to misfolding, as protein crystals of the R971A mutant were obtained under standard conditions (unpublished observation). The role of R971 might be analogous to that of bacteriorhodopsin's R82, which is engaged in a hydrogen bonding network with coordinated water molecules and polar and charged side chains (*60*). Recent work postulates (partial) deprotonation of R82, which might be valid for AcrB R971 as well (*61*).

DISCUSSION

All studied proton translocation pathways in primary and secondary active transporters include key carboxylates, which are essential for function (*33*, *34*, *62*−*64*). Most of these carboxylates are located in a hydrophobic environment, and their pK_a values are, at least at some stage of the transport cycle, close to physiological pH which allows protonation−deprotonation reactions to occur. The proton translocation pathways of bacteriorhodopsin and cytochrome *c* oxidase are studied in detail, because the pK_a values of key carboxylates could be determined by time-resolved spectroscopy using the advantage of excitable intrinsic chromophores (*65*−*67*). Other systems such as LacY, EmrE, and F_1F_o ATPase were studied by specific labeling of these carboxylates using hydrophobic carbodiimides (*38*−*40*, *50*, *68*). DCCD labeling on secondary transporters LacY (*39*) and EmrE (*40*) was studied by electrospray ionization mass spectrometry (ESI-MS). In this report, we combined carbodiimide labeling with mass spectrometry analysis of CNBr-digested AcrB, which proved to be a powerful tool for locating titratable carboxylates and for estimating their pK_a values. We determined the carbodiimide modification of AcrB by quantitative MALDI-TOF (*69*, *70*), using peak intensities of unmodified peptides as the internal standard. Analysis by MALDI-TOF/TOF allowed the identification of one single carboxylate, D408, as being specifically reactive to DCCD within the transmembrane domain of wild-type AcrB. Its pK_a was determined to be 7.4, which allows protonation−deprotonation reactions to occur at physiological pH. These data fit well with the proposed H^+ binding and release and the side chain conformations of these residues within the AcrB asymmetric structure.

As illustrated in Figure 6, in the L and T monomer, K940 resides between D407 and D408, whereas K940 undergoes a substantial side chain adjustment toward D407 and T978 in the O monomer. In this conformation, the distance between D408 and K940 is greater than 8 Å and D408 appears to be hydrogen bonded with the backbone carbonyl of L442 (distance of 2.8 Å). In our proposed model (Figure 6), the O monomer contains protonated D407 and D408. In the T momomer, both these aspartates are postulated to be deprotonated. For the L monomer, we depicted a protonated D408 and deprotonated D407; however, we considered alternatively also two deprotonated species of D407 and D408. D408 is therefore postulated to be protonated in the O and alternatively also in the L monomer. Since carbodiimide labeling occurs only at protonated carboxylates, we reason that D408 becomes labeled in the O and/or the L monomer. DCCD labeling experiments with AcrB solubilized in CHM or DDM (i.e., in the absence of LDAO) resulted in a maximal level of labeling of 30% of all AcrB molecules. One explanation would be that D408 is only reactive in one monomer, which might be, e.g., the O monomer because of the distance between K940 and D408 and the relative isolation of D408 in a hydrophobic environment (Figure 6). However, since CHM- or DDM-solubilized AcrB is prone to aggregation after DCCD incubation, this interpretation has to be taken with much caution. The presence of LDAO (0.1%) dramatically increases labeling efficiency to > 80%, and it also prohibits precipitation. The effect by LDAO is likely to be due to its properties as a detergent, although direct interaction of the *N*-oxide group in the DCCD labeling reaction cannot be excluded. The results might also suggest that the LDAO-stimulated labeling is caused by uncoupling of the LTO assembly or stimulates the presence of other trimeric states next to LTO (*24*, *25*) like LLL (*20*). Despite the uncertainty regarding the stoichiometry of DCCD labeling at D408, the specific labeling at D408 in wild-type AcrB is an interesting observation per se. We propose that D408 plays a crucial role in proton binding and release, which can be accomplished at physiological pH. Interestingly, the D408N mutant still confers low but clearly measurable drug resistance, whereas the D407N mutant is completely nonfunctional (Table 1). This could indicate an assisting role of D408 in the timely acquisition or release of protons which are passed on to or taken up from indispensible D407. Our efforts to test functional DCCD inhibition of AcrB within the frame of a fluorescent assay in a whole cell system were stranded at the level of interpretation of the results, since concomitant inhibition of the respiratory chain affects the extent of the proton motive force and thereby indirectly the pumping activity of the AcrAB-TolC efflux pump.

Substrates were reported to protect the specific carboxylate on the protein from labeling with DCCD; e.g., the rate of carbodiimide modification of the secondary active tranporters LacY and EmrE was significantly decreased in the presence of the cognate substrates *p*-nitrophenyl-α-D-galactopyranoside and tetraphenylphosphonium, respectively (*39*, *40*). The labeling protection was interpreted as a competition of drugs and protons for interaction with the same carboxylates. In these typical secondary transporters, a dual role inheres to key carboxylates, namely, the interaction with substrates and the translocation of protons (*39*, *40*). On the basis of functional and structural studies, AcrB is suggested to exhibit spatially separated paths for drugs (at the periplasmic loops) and protons (at the transmembrane domain) (*24*, *25*, *29*−*31*). On the other hand, the possible transport of drugs from the cytoplasmic to the periplasmic membrane leaflet of the inner membrane by AcrB is a long-standing proposal, although direct biochemical evidence is lacking thus far (*1*, *59*, *71*). Here, we provide for the first time indirect evidence that drugs which are known to be transported by AcrB do not seem to interact with the key carboxylate D408 suggested to play a central role in proton translocation (Figure 4d). In case transport across the inner membrane would be mediated by AcrB for the drugs tested, our result would at least be indicative of no direct interaction between the drugs and the residues involved in proton translocation, supporting the notion of spatial separation of substrate and proton transport pathways. In analogy to ABC transporters or P-type ATPases, conformational changes at the site of energy input (ABC cassettes in the case of ABC transporters or a membrane-embedded charged network in case of AcrB) are coupled to conformational changes in distant domains where the substrate transport takes place (*72*, *73*).

In the proposed functional rotation cycle (*24*, *25*), the conversion of the T monomer to the O monomer results in movement of K940 away from the putatively unprotonated D407/D408 pair toward T978, S979, and N941. Intriguingly, the upward movement of D407 and the bulging of TM5 toward D408 bring both side chains into a very hydrophobic environment, which might

result in an increase in their pK_a values and binding of protons from the periplasm (Figure 6). It is suggested that K940 is deprotonated during the T to O monomer conversion on the basis of the observation that each of the residues comprising the ε-amino group's polar environment (T978, S979, and N941) can be substituted with alanine, or in the case of T978 with valine, without a dramatic loss of activity.

In summary, D407 and D408 are at the center of an elaborate charge network responsible for the timely binding and release of protons, which is most probably coupled to the binding and extrusion of drugs in the porter domain. K940 might play the role of a switch, which imposes the direction of structural conversions, similar to the Schiff base nitrogen of the bacteriorhodopsin (*33*). The distance from the amine group of K940 to the carboxyl moieties of D407 and D408 changes drastically along the transport cycle which strongly influences the pK_a values of not only these carboxylates but also K940 itself. R971 finally is proposed to play a key role in the pathway from the triad to the cytoplasm by influencing the pK_a of D407 or the orientation of putative structural water molecules between these residues. In all three monomers, R971 movement correlates with F948 side chain movement. Distances between these residues in every monomer are ~4 Å; i.e., cation$-\pi$ interactions might be feasible. Analogous to recent work on bacteriodopsin's R82 (*61*), partial deprotonation might occur at R971 presumably in the L monomer (Figure 6) (*4*, *74*).

The question of how protons can overbear a distance greater than 10 Å through hydrophobic space between the periplasm and the proton translocation site in the T monomer remains elusive. The highest-resolution crystal structure of asymmetric AcrB at 2.5 Å resolution (*26*) does not allow the unambiguous allocation of structural water molecules in the transmembrane domain of AcrB. Hydrophobic barriers are a common feature of ion translocation pathways found as well in bacteriorhodopsin (*33*), cytochrome *c* oxidase (*34*), or the F_1F_o ATP synthase (*75*).

In summary, carbodiimide labeling, mutational analysis, and the asymmetric structure support the central role of the charged residues constituting the triad in the proton translocation pathway, which appears to be spatially separated from the efflux pathway of the drugs.

ACKNOWLEDGMENT

MALDI-TOF measurements were performed at the Functional Genomics Center Zurich (FGCZ). We thank P. Gehrig from the FGCZ for assistance with the MALDI-TOF instrument.

SUPPORTING INFORMATION AVAILABLE

Figures 1 and 2. This material is available free of charge via the Internet at http://pubs.acs.org.

REFERENCES

1. Nikaido, H. (1996) Multidrug efflux pumps of Gram-negative bacteria. *J. Bacteriol. 178*, 5853–5859.
2. Murakami, S. (2008) Multidrug efflux transporter, AcrB: The pumping mechanism. *Curr. Opin. Struct. Biol. 18*, 459–465.
3. Lomovskaya, O., Zgurskaya, H. I., Totrov, M., and Watkins, W. J. (2007) Waltzing transporters and 'the dance macabre' between humans and bacteria. *Nat. Rev. Drug Discovery 6*, 56–65.
4. Seeger, M. A., Diederichs, K., Eicher, T., Brandstatter, L., Schiefner, A., Verrey, F., and Pos, K. M. (2008) The AcrB Efflux Pump: Conformational Cycling and Peristalsis Lead to Multidrug Resistance. *Curr. Drug Targets 9*, 729–749
5. Zgurskaya, H. I., and Nikaido, H. (1999) Bypassing the periplasm: Reconstitution of the AcrAB multidrug efflux pump of *Escherichia coli*. *Proc. Natl. Acad. Sci. U.S.A. 96*, 7190–7195
6. Ma, D., Cook, D. N., Alberti, M., Pon, N. G., Nikaido, H., and Hearst, J. E. (1993) Molecular cloning and characterization of acrA and acrE genes of *Escherichia coli*. *J. Bacteriol. 175*, 6299–6313
7. Fralick, J. A. (1996) Evidence that TolC is required for functioning of the Mar/AcrAB efflux pump of *Escherichia coli*. *J. Bacteriol. 178*, 5803–5805
8. Tikhonova, E. B., and Zgurskaya, H. I. (2004) AcrA, AcrB, and TolC of *Escherichia coli* Form a Stable Intermembrane Multidrug Efflux Complex. *J. Biol. Chem. 279*, 32116–32124
9. Touze, T., Eswaran, J., Bokma, E., Koronakis, E., Hughes, C., and Koronakis, V. (2004) Interactions underlying assembly of the *Escherichia coli* AcrAB-TolC multidrug efflux system. *Mol. Microbiol. 53*, 697–706
10. Husain, F., Humbard, M., and Misra, R. (2004) Interaction between the TolC and AcrA proteins of a multidrug efflux system of *Escherichia coli*. *J. Bacteriol. 186*, 8533–8536
11. Tamura, N., Murakami, S., Oyama, Y., Ishiguro, M., and Yamaguchi, A. (2005) Direct interaction of multidrug efflux transporter AcrB and outer membrane channel TolC detected via site-directed disulfide cross-linking. *Biochemistry 44*, 11115–11121
12. Stegmeier, J. F., Polleichtner, G., Brandes, N., Hotz, C., and Andersen, C. (2006) Importance of the adaptor (membrane fusion) protein hairpin domain for the functionality of multidrug efflux pumps. *Biochemistry 45*, 10303–10312
13. Bokma, E., Koronakis, E., Lobedanz, S., Hughes, C., and Koronakis, V. (2006) Directed evolution of a bacterial efflux pump: Adaptation of the *E. coli* TolC exit duct to the *Pseudomonas* MexAB translocase. *FEBS Lett. 580*, 5339–5343
14. Lobedanz, S., Bokma, E., Symmons, M. F., Koronakis, E., Hughes, C., and Koronakis, V. (2007) A periplasmic coiled-coil interface underlying TolC recruitment and the assembly of bacterial drug efflux pumps. *Proc. Natl. Acad. Sci. U.S.A. 104*, 4612–4617
15. Okusu, H., Ma, D., and Nikaido, H. (1996) AcrAB efflux pump plays a major role in the antibiotic resistance phenotype of *Escherichia coli* multiple-antibiotic-resistance (Mar) mutants. *J. Bacteriol. 178*, 306–308.
16. Poole, K. (2000) Efflux-mediated resistance to fluoroquinolones in Gram-negative bacteria. *Antimicrob. Agents Chemother. 44*, 2233–2241.
17. Koronakis, V., Sharff, A., Koronakis, E., Luisi, B., and Hughes, C. (2000) Crystal structure of the bacterial membrane protein TolC central to multidrug efflux and protein export. *Nature 405*, 914–919.
18. Akama, H., Kanemaki, M., Yoshimura, M., Tsukihara, T., Kashiwagi, T., Yoneyama, H., Narita, S., Nakagawa, A., and Nakae, T. (2004) Crystal structure of the drug discharge outer membrane protein, OprM, of *Pseudomonas aeruginosa*: Dual modes of membrane anchoring and occluded cavity end. *J. Biol. Chem. 279*, 52816–52819.
19. Mikolosko, J., Bobyk, K., Zgurskaya, H. I., and Ghosh, P. (2006) Conformational flexibility in the multidrug efflux system protein AcrA. *Structure 14*, 577–587.
20. Murakami, S., Nakashima, R., Yamashita, E., and Yamaguchi, A. (2002) Crystal structure of bacterial multidrug efflux transporter AcrB. *Nature 419*, 587–593.
21. Pos, K. M., and Diederichs, K. (2002) Purification, crystallization and preliminary diffraction studies of AcrB, an inner-membrane multidrug efflux protein. *Acta Crystallogr. D58*, 1865–1867.
22. Pos, K. M., Schiefner, A., Seeger, M. A., and Diederichs, K. (2004) Crystallographic analysis of AcrB. *FEBS Lett. 564*, 333–339.
23. Yu, E. W., McDermott, G., Zgurskaya, H. I., Nikaido, H., and Koshland, D. E.Jr. (2003) Structural basis of multiple drug-binding capacity of the AcrB multidrug efflux pump. *Science 300*, 976–980.
24. Seeger, M. A., Schiefner, A., Eicher, T., Verrey, F., Diederichs, K., and Pos, K. M. (2006) Structural asymmetry of AcrB trimer suggests a peristaltic pump mechanism. *Science 313*, 1295–1298.
25. Murakami, S., Nakashima, R., Yamashita, E., Matsumoto, T., and Yamaguchi, A. (2006) Crystal structures of a multidrug transporter reveal a functionally rotating mechanism. *Nature 443*, 173–179.
26. Sennhauser, G., Amstutz, P., Briand, C., Storchenegger, O., and Grutter, M. G. (2006) Drug Export Pathway of Multidrug Exporter AcrB Revealed by DARPin Inhibitors. *PLoS Biol. 5*, e7.
27. Guan, L., and Nakae, T. (2001) Identification of essential charged residues in transmembrane segments of the multidrug transporter MexB of *Pseudomonas aeruginosa*. *J. Bacteriol. 183*, 1734–1739
28. Takatsuka, Y., and Nikaido, H. (2006) Threonine-978 in the transmembrane segment of the multidrug efflux pump AcrB of *Escherichia coli* is crucial for drug transport as a probable component of the proton relay network. *J. Bacteriol. 188*, 7284–7289
29. Tikhonova, E. B., Wang, Q., and Zgurskaya, H. I. (2002) Chimeric analysis of the multicomponent multidrug efflux transporters from Gram-negative bacteria. *J. Bacteriol. 184*, 6499–6507.

30. Elkins, C. A., and Nikaido, H. (2002) Substrate specificity of the RND-type multidrug efflux pumps AcrB and AcrD of *Escherichia coli* is determined predominantly by two large periplasmic loops. *J. Bacteriol. 184*, 6490–6498.
31. Eda, S., Maseda, H., and Nakae, T. (2003) An elegant means of self-protection in Gram-negative bacteria by recognizing and extruding xenobiotics from the periplasmic space. *J. Biol. Chem. 278*, 2085–2088.
32. Su, C. C., Li, M., Gu, R., Takatsuka, Y., McDermott, G., Nikaido, H., and Yu, E. W. (2006) Conformation of the AcrB multidrug efflux pump in mutants of the putative proton relay pathway. *J. Bacteriol. 188*, 7290–7296.
33. Lanyi, J. K. (2004) Bacteriorhodopsin. *Annu. Rev. Physiol. 66*, 665–688.
34. Hosler, J. P., Ferguson-Miller, S., and Mills, D. A. (2006) Energy Transduction: Proton Transfer Through the Respiratory Complexes. *Annu. Rev. Biochem. 75*, 165–187.
35. Venter, H., Shahi, S., Balakrishnan, L., Velamakanni, S., Bapna, A., Woebking, B., and van Veen, H. W. (2005) Similarities between ATP-dependent and ion-coupled multidrug transporters. *Biochem. Soc. Trans. 33*, 1008–1011.
36. Miller, M. J., Oldenburg, M., and Fillingame, R. H. (1990) The essential carboxyl group in subunit c of the F1F0 ATP synthase can be moved and H^+-translocating function retained. *Proc. Natl. Acad. Sci. U.S.A. 87*, 4900–4904.
37. von Ballmoos, C., Meier, T., and Dimroth, P. (2002) Membrane embedded location of Na^+ or H^+ binding sites on the rotor ring of F1F0 ATP synthases. *Eur. J. Biochem. 269*, 5581–5589.
38. von Ballmoos, C., and Dimroth, P. (2007) Two distinct proton binding sites in the ATP synthase family. *Biochemistry 46*, 11800–11809.
39. Weinglass, A. B., Whitelegge, J. P., Hu, Y., Verner, G. E., Faull, K. F., and Kaback, H. R. (2003) Elucidation of substrate binding interactions in a membrane transport protein by mass spectrometry. *EMBO J. 22*, 1467–1477.
40. Weinglass, A. B., Soskine, M., Vazquez-Ibar, J. L., Whitelegge, J. P., Faull, K. F., Kaback, H. R., and Schuldiner, S. (2005) Exploring the role of a unique carboxyl residue in EmrE by mass spectrometry. *J. Biol. Chem. 280*, 7487–7492.
41. Sambrook, J., Fritsch, E. F., and Maniatis, T. (1989) Molecular cloning: Alaboratory manual , Cold Spring Harbor Laboratory Press, Plainview, NY.
42. Inoue, H., Nojima, H., and Okayama, H. (1990) High efficiency transformation of *Escherichia coli* with plasmids. *Gene 96*, 23–28.
43. Miroux, B., and Walker, J. E. (1996) Over-production of proteins in *Escherichia coli*: Mutant hosts that allow synthesis of some membrane proteins and globular proteins at high levels. *J. Mol. Biol. 260*, 289–298.
44. Kraft, P., Mills, J., and Dratz, E. (2001) Mass spectrometric analysis of cyanogen bromide fragments of integral membrane proteins at the picomole level: Application to rhodopsin. *Anal. Biochem. 292*, 76–86.
45. von Ballmoos, C., Appoldt, Y., Brunner, J., Granier, T., Vasella, A., and Dimroth, P. (2002) Membrane topography of the coupling ion binding site in Na^+-translocating F_1F_0 ATP synthase. *J. Biol. Chem. 277*, 3504–3510.
46. Khorana, H. G. (1953) The Chemistry of Carbodiimides. *Chem. Rev. 53*, 145–166.
47. Kaiser, R., and Metzka, L. (1999) Enhancement of cyanogen bromide cleavage yields for methionyl-serine and methionyl-threonine peptide bonds. *Anal. Biochem. 266*, 1–8.
48. Wysocki, V. H., Tsaprailis, G., Smith, L. L., and Breci, L. A. (2000) Mobile and localized protons: A framework for understanding peptide dissociation. *J. Mass Spectrom. 35*, 1399–1406.
49. Kluge, C., and Dimroth, P. (1993) Specific protection by Na^+ or Li^+ of the F1F0-ATPase of *Propionigenium modestum* from the reaction with dicyclohexylcarbodiimide. *J. Biol. Chem. 268*, 14557–14560.
50. Meier, T., Matthey, U., von Ballmoos, C., Vonck, J., Krug von Nidda, T., Kuhlbrandt, W., and Dimroth, P. (2003) Evidence for structural integrity in the undecameric c-rings isolated from sodium ATP synthases. *J. Mol. Biol. 325*, 389–397.
51. Su, C. C., and Yu, E. W. (2007) Ligand-transporter interaction in the AcrB multidrug efflux pump determined by fluorescence polarization assay. *FEBS Lett. 581*, 4972–4976.
52. Weinglass, A. B., Sondej, M., and Kaback, H. R. (2002) Manipulating conformational equilibria in the lactose permease of *Escherichia coli*. *J. Mol. Biol. 315*, 561–571
53. Saier, M. H.Jr., and Paulsen, I. T. (2001) Phylogeny of multidrug transporters. *Semin. Cell Dev. Biol. 12*, 205–213
54. Guan, L., and Kaback, H. R. (2006) Lessons from lactose permease. *Annu. Rev. Biophys. Biomol. Struct. 35*, 67–91
55. Kim, S. H., Chang, A. B., and Saier, M. H.Jr. (2004) Sequence similarity between multidrug resistance efflux pumps of the ABC and RND superfamilies. *Microbiology 150*, 2493–2495
56. Ernst, R., Kueppers, P., Klein, C. M., Schwarzmueller, T., Kuchler, K., and Schmitt, L. (2008) A mutation of the H-loop selectively affects rhodamine transport by the yeast multidrug ABC transporter Pdr5. *Proc. Natl. Acad. Sci. U.S.A. 105*, 5069–5074
57. Rammelsberg, R., Huhn, G., Lubben, M., and Gerwert, K. (1998) Bacteriorhodopsin's intramolecular proton-release pathway consists of a hydrogen-bonded network. *Biochemistry 37*, 5001–5009
58. Goldberg, M., Pribyl, T., Juhnke, S., and Nies, D. H. (1999) Energetics and topology of CzcA, a cation/proton antiporter of the resistance-nodulation-cell division protein family. *J. Biol. Chem. 274*, 26065–26070
59. Murakami, S., and Yamaguchi, A. (2003) Multidrug-exporting secondary transporters. *Curr. Opin. Struct. Biol. 13*, 443–452
60. Balashov, S. P., Govindjee, R., Kono, M., Imasheva, E., Lukashev, E., Ebrey, T. G., Crouch, R. K., Menick, D. R., and Feng, Y. (1993) Effect of the arginine-82 to alanine mutation in bacteriorhodopsin on dark adaptation, proton release, and the photochemical cycle. *Biochemistry 32*, 10331–10343
61. Xiao, Y., Hutson, M. S., Belenky, M., Herzfeld, J., and Braiman, M. S. (2004) Role of arginine-82 in fast proton release during the bacteriorhodopsin photocycle: A time-resolved FT-IR study of purple membranes containing ^{15}N-labeled arginine. *Biochemistry 43*, 12809–12818
62. Dimroth, P., von Ballmoos, C., and Meier, T. (2006) Catalytic and mechanical cycles in F-ATP synthases. Fourth in the Cycles Review Series. *EMBO Rep. 7*, 276–282
63. Olkhova, E., Hunte, C., Screpanti, E., Padan, E., and Michel, H. (2006) Multiconformation continuum electrostatics analysis of the NhaA Na^+/H^+ antiporter of *Escherichia coli* with functional implications. *Proc. Natl. Acad. Sci. U.S.A. 103*, 2629–2634
64. Guan, L., and Kaback, H. R. (2005) Lessons from Lactose Permease. *Annu. Rev. Biophys. Biomol. Struct. 35*, 67–91
65. Balashov, S. P., Imasheva, E. S., Govindjee, R., and Ebrey, T. G. (1996) Titration of aspartate-85 in bacteriorhodopsin: What it says about chromophore isomerization and proton release. *Biophys. J. 70*, 473–481
66. Namslauer, A., and Brzezinski, P. (2004) Structural elements involved in electron-coupled proton transfer in cytochrome c oxidase. *FEBS Lett. 567*, 103–110
67. Garczarek, F., and Gerwert, K. (2006) Polarized FTIR spectroscopy in conjunction with in situ H/D exchange reveals the orientation of protein internal carboxylic acids. *J. Am. Chem. Soc. 128*, 28–29
68. Kluge, C., and Dimroth, P. (1993) Kinetics of inactivation of the F_1F_o ATPase of *Propionigenium modestum* by dicyclohexylcarbodiimide in relationship to H^+ and Na^+ concentration: Probing the binding site for the coupling ions. *Biochemistry 32*, 10378–10386
69. Gobom, J., Kraeuter, K. O., Persson, R., Steen, H., Roepstorff, P., and Ekman, R. (2000) Detection and quantification of neurotensin in human brain tissue by matrix-assisted laser desorption/ionization time-of-flight mass spectrometry. *Anal. Chem. 72*, 3320–3326.
70. Helmke, S. M., Yen, C. Y., Cios, K. J., Nunley, K., Bristow, M. R., Duncan, M. W., and Perryman, M. B. (2004) Simultaneous quantification of human cardiac α- and β-myosin heavy chain proteins by MALDI-TOF mass spectrometry. *Anal. Chem. 76*, 1683–1689.
71. Das, D., Xu, Q. S., Lee, J. Y., Ankoudinova, I., Huang, C., Lou, Y., DeGiovanni, A., Kim, R., and Kim, S. H. (2007) Crystal structure of the multidrug efflux transporter AcrB at 3.1 Å resolution reveals the N-terminal region with conserved amino acids. *J. Struct. Biol. 158*, 494–502.
72. Kuhlbrandt, W. (2004) Biology, structure and mechanism of P-type ATPases. *Nat. Rev. Mol. Cell Biol. 5*, 282–295.
73. Dawson, R. J., and Locher, K. P. (2006) Structure of a bacterial multidrug ABC transporter. *Nature 443*, 180–185.
74. Pos, K. M. (2009) Drug transport mechanism of the AcrB efflux pump. *Biochim. Biophys. Acta* (in press).
75. Meier, T., Polzer, P., Diederichs, K., Welte, W., and Dimroth, P. (2005) Structure of the rotor ring of F-Type Na^+-ATPase from *Ilyobacter tartaricus*. *Science 308*, 659–662.
76. Seeger, M. A., von Ballmoos, C., Eicher, T., Brandstätter, L., Verrey, F., Diederichs, K., and Pos, K. M. (2008) Engineered disulfide bonds support the functional rotation mechanism of multidrug efflux pump AcrB. *Nat. Struct. Mol. Biol. 15*, 199–205.